Processing and Application of Ceramics 16 [1] (2022) 69–77
https://doi.org/10.2298/PAC2201069B

High-temperature evolution of diamond-SiC composites

Eszter Bódis[1,*], Ildikó Cora[2], Zsolt Fogarassy[2], Miklós Veres[3], Péter Németh[4,5]

[1]*Institute of Materials and Environmental Chemistry, Research Centre for Natural Sciences, Eötvös Loránd Research Network, H-1117 Budapest, Magyar Tudósok körútja 2, Hungary*
[2]*Institute of Technical Physics and Materials Science, Centre for Energy Research, Eötvös Loránd Research Network, H-1121 Budapest, Konkoly-Thege Miklós út 29-33, Hungary*
[3]*Institute for Solid State Physics and Optics, Wigner Research Centre for Physics, Eötvös Loránd Research Network, H- 1121 Budapest, Konkoly-Thege Miklós út 29-33, Hungary*
[4]*Institute for Geological and Geochemical Research, Research Centre for Astronomy and Earth Sciences, Eötvös Loránd Research Network, H-1112 Budapest Budaörsi út 45, Hungary*
[5]*Department of Earth and Environmental Sciences, University of Pannonia, H-8200, Veszprém Egyetem út 10, Hungary*

Received 14 October 2021; Received in revised form 21 January 2022; Accepted 21 February 2022

Abstract

Diamond-SiC composites are attractive for improving the catastrophic fracture behaviour of SiC. However, fundamental knowledge is missing about the structure of this system and the mechanism of diamond graphitization. We used spark plasma sintering to study the diamond-Si-SiC system between 1600 and 2000 °C in the function of nanocrystalline (ND) and microcrystalline (MD) diamond addition as well as the quantity of Si-bonding phase. Increasing sintering temperature induces intense graphitization and formation of nano-onions, few-layered graphene and well-ordered graphite in the prepared composites at elevated temperature. High resolution transmission electron microscopy study demonstrates the occurrence of the previously erroneously identified 5H-SiC polytype in the samples prepared at 2000 °C. Regardless of Si and diamond contents, SiC formation is not confirmed even at high temperature.

Keywords: *SiC-diamond composites, nanosized and microsized diamond, SPS, 5H-SiC phase*

I. Introduction

Nanodiamonds (NDs) are in the focus of intense interdisciplinary research [1–4]. For example fluorescent NDs can be applied as non-toxic semiconductor quantum dots for biomedical imaging [2]. Their homogeneous small (~3 nm) size and narrow distribution, chemical inertness and facile surface functionalization offer wide possibilities for applications in biomedical research, with special attention to nanofabrication and drug delivery [5–8]. The exceptionally high hardness, strength and wear resistance enable their use for various applications including hard and resistant coatings [1,9] and even as additives in engine motor oils [10]. NDs are also attractive as reinforcing materials since diamond particles incorporated into metals [11,12], ceramics [13,14] or graphene [15,16] matrix can enhance the thermal and mechanical properties of the resulting composites.

Silicon carbide (SiC), similarly to diamond, has excellent physical and chemical properties, such as high hardness, high thermal conductivity, high wear and corrosion resistance, as well as low thermal expansion [17]. However, it is rather rigid and has catastrophic fracture behaviour, which can be improved by the addition of multilayer graphene [18] or ZrO_2 nanofibre [19]. Since diamond has the highest fracture resistance its addition to SiC can also be a promising way to improve the fracture behaviour of SiC and thus to synthesize SiC-diamond composites for preparing super-hard cutting tools.

The main synthesis route to fabricate SiC-diamond composites is the so-called reactive Si infiltration technique at high-pressure and high-temperature (HTHP). During this preparation SiC forms as a result of the

* Corresponding author: tel: +36 1 3826505,
e-mail: *bodis.eszter@ttk.hu*

in-situ diffusion-reaction between silicon and microdiamond (MD) [20]. These composites show good mechanical properties thanks to the *in-situ* formed SiC, which can strongly bond the reinforced phase and the matrix [21]. However, this method requires a very large amount (80–90 vol.%) of diamond addition, since it is the carbon source for the evolving SiC and the multistep infiltration. The requirement of the large amount of diamond addition and the difficult experimental infiltration procedure can be avoided by the simple mixing of SiC, diamond and Si as a bonding phase. However, during such synthesis there is no *in-situ* reaction, and thus unreacted Si can remain and can degrade the mechanical and thermal properties of the composite [22,23].

Since nanostructured materials show more distinct properties than micro-sized ones, the question arises how the nanocrystalline diamond addition into SiC matrix can influence the physical and chemical features of the composite. Although this question has been addressed in a few studies [24–27], fundamental knowledge is missing about the behaviour of the SiC-Si-diamond system. In particular, the size of the added diamond (nano or micro), the graphitization mechanisms of diamond and the role of the bonding phase during the procedure have been poorly investigated.

Here, we fabricate SiC-diamond composites applying the spark plasma sintering (SPS) technique, which offers the advantage of very fast heat treatment with high heating and cooling rates compared with those of conventional sintering techniques. Due to the rapid heat treatment of diamond, it is expected that the graphitization of diamond may be reduced. Our aim is to study the SiC-Si-diamond system by focusing on the effect of nano- and microcrystalline diamond addition as well as the influence of the silicon quantity in order to better understand the interface properties.

II. Experimental procedure

2.1. Sample preparation

The starting materials were commercial SiC (Washington Mills, average grain size of 3 μm), diamond ND (ACS Materials type DINP0125/ Szkarabeusz Ltd, average particle size of 50 nm) and diamond MD (Szkarabeusz Ltd, average particle size of 3 μm) powders. Following the general concept that even low amount of additive can significantly influence the sinterability and physical properties of the compounds, we prepared different SiC-Si-diamond composites (SiC-ND and SiC-MD - Table 1).

For preparing the SiC-ND composites, the SiC particles were coated with nanosize Si layer using radio frequency sputtering deposition system. Before the sputtering process, the SiC particles were cleaned with 4 wt.% HF solution in order to reduce the SiO_2 content on the SiC surface. For the nanoscale Si deposition, 99% pure Si target was used in an A300 magnetron sputtering deposition system made by AJA International operating at high vacuum (10^{-5} Pa). Argon gas was poured into the chamber to maintain the constant pressure of 1 Pa. 20 W power has been applied to Si target. Si has been deposited on 1 g SiC for 60 min. After the sputtering procedures, the SiC powder containing ~1 wt.% Si (calculated from weight of the starting and the as-sputtered SiC) was produced. The ultrafine ND was suspended in 99.97% absolute ethanol (99.97%, Molar Chemical) and then sonicated by high-efficiency ultrasound equipment for 60 min in order to obtain the most homogeneous diamond distribution. The Si covered SiC powder was mixed with the ND suspension to obtain mixture with 10 wt.% ND, 89 wt.% SiC and 1 wt.% Si. The suspension was stirred continuously at 80 °C to remove the excess ethanol and to avoid the undesirable sedimentation of the components. As a result, a highly concentrated suspension was obtained, which was completely dried at 90 °C for 24 h. For comparison addition-free SiC and Si covered SiC reference samples were prepared.

The SiC-MD composites were also obtained from the SiC powder cleaned with 4 wt.% HF solution. The cleaned SiC was mixed with 10 wt.% Si powder (Sigma-Aldrich, average particle size of 3 μm) and ball-milled in absolute ethanol. In the same time, 5 wt.% micrometre-sized MD diamond powder (having the same average particle size as that of SiC and Si powders) was sus-

Table 1. Experimental conditions

Composites	Sintering temperature [°C]	Composition [%] SiC	Si	diamond
SiC-ND composite	1600	100	0	0
		99	1	
		90	0	10
		89	1	
	1800	100	0	0
		99	1	
		90	0	10
		89	1	
SiC-MD composite	1600	85	10	5
	1800			
	2000			
	2000	90	10	0

pended in absolute ethanol and then sonicated by high-efficiency ultrasound equipment for 60 min. After sonication, the SiC-Si mixture was added to the diamond suspension, and the mixture was stirred continuously at 80 °C to remove most of ethanol. The highly concentrated suspension was completely dried at 90 °C for 24 h. Reference sample of diamond- free SiC containing 10 wt.% Si powder mixtures was also prepared. Compositions of these mixtures are given in Table 1.

2.2. Sintering conditions

The various powder mixtures were heat treated by a HPD25 SPS equipment supplied by the FCT System GmbH (Germany) at 10^{-2} mbar vacuum. In order to understand structural evolutions in SiC-Si-diamond system including the graphitization of diamonds, the mixtures were sintered at relatively low 1600 °C and at extremely high temperatures (at 1800 and 2000 °C) with 100 °C/min heating rate and 5 min dwell time at maximum temperature. During the heat treatment, the applied pressure was 50 MPa. The sintered bodies had 20 mm diameter. The experimental conditions are summarized in Table 1.

2.3. Characterization methods

Phase compositions of the samples were characterized by X-ray diffraction (X'Pert, PANalytical B.V.) using Cu Kα radiation in 2θ range of 10 to 70° with 0.04° step for 1 s. The composite bodies were analysed by Raman spectroscopy in order to obtain information about the different carbon structures in the composites. Raman spectra of the heat treated samples were collected in a Reinshaw InVia micro-Raman spectrometer equipped with a CCD detector. A green laser (λ = 532 nm) was focused (2 μm diameter spot) on the composite surface using an optical microscope (Leica DM2700) coupled with the spectrometer. Spectra were recorded after 20 s exposure time. Curve fitting of the Raman data was carried out using Origin 8.0 software and the detected Raman bands were identified based on the literature data [28].

Microstructure and morphology of the composites bodies were analysed by scanning (SEM, ZEISS LEO 1540 XB) and transmission electron microscopy (TEM, CM-20). For a detailed nanostructural characterization a FEI Themis microscope was used (operated on 200 kV). We obtained bright-field (BFTEM), high-resolution (HRTEM) and high-angle annular dark-field (HAADF) images as well as selected area diffraction (SAED) patterns. The chemical composition of the grains was measured with a "Super-X" detector system having four Si drift detectors (SDD) built into the microscope. The Fast Fourier transform was calculated using the Gatan Digital Micrograph 3.6.1 software. For the TEM observations, the samples were initially mechanically thinned, dimpled and thinned by Ar-ion to electron transparency. Finally, a Gentle Mill instrument (Technoorg Linda) was used to remove the bombarded layers.

III. Results and discussion

3.1. Phase composition

X-ray diffraction analysis was used to follow up the phase changes in the SiC-ND and SiC-MD composites during sintering (Fig. 1). Comparing the initial phase composition with the compositions of the sintered SiC-ND samples, the most obvious modification occurred for diamond phase. In the SiC-ND samples even at low sintering temperature (at 1600 °C) diamond phase was transformed to nanographite, which is evidenced by graphite XRD peak at 2θ at ~23°. XRD peaks of Si were invisible in the Si-sputtered composites. Comparing the phase composition of the Si containing and Si-free SiC-ND samples, we did not observe that Si addition influenced the diamond transformation.

For the SiC-MD samples containing large amount (10 wt.%) of Si addition, XRD measurements showed that diamond phase still occurs after sintering at 1600 and 1800 °C (Fig. 1b). However, its amount decreases continuously with the increasing temperature and at

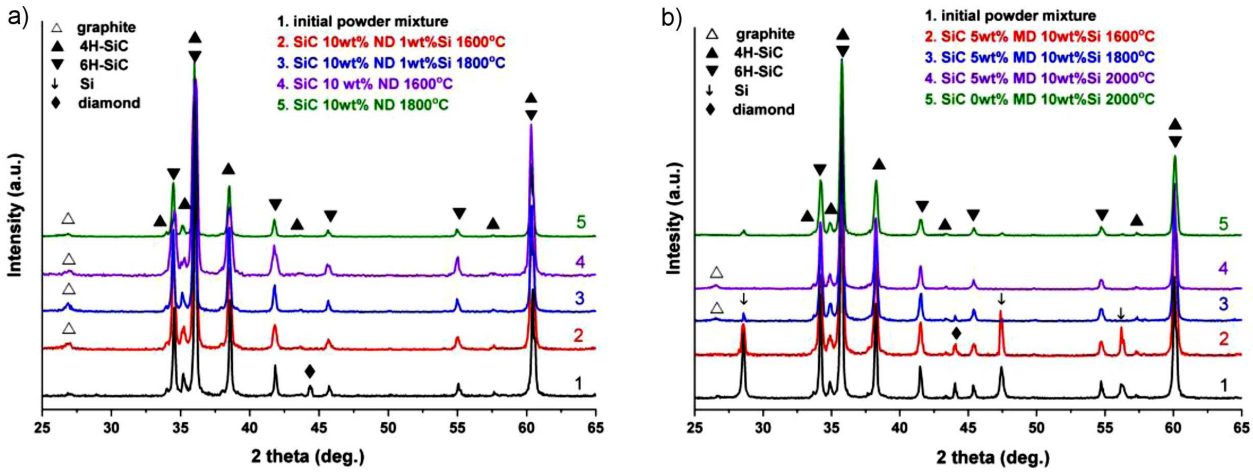

Figure 1. XRD patterns of: a) SiC-ND and b) SiC-MD samples obtained by various sintering conditions

maximal sintering temperate (2000 °C) diamond phase was transformed into graphite. The decreased amount of Si at 1800 °C and the lack of Si at 2000 °C could be associated with the inhomogeneous Si distribution, because in the 10 wt.% Si containing MD-free SiC composite the Si peak was evident (Fig. 1b).

We conclude that the quantity of the Si sintering additive does not influence the structural transformation of nanosized (ND) and microsized diamond (MD) phases. According to the relevant literature reports Si should have reacted with diamond resulting in SiC. However, we found that Si and diamond did not form SiC as Si and graphite occurred as separate phases even at high temperature (2000 °C).

3.2. Morphology

In order to study the influence of Si addition on microstructure of the SiC-ND system, the fractured surfaces of the pure and Si-sputtered SiC samples were analysed using SEM (Fig. 2). The sputtered Si was not obviously detectable on the surface of SiC grains of the sample sintered at 1600 °C. Furthermore, the added Si did not influence the densification of the composites since the pure SiC and Si-sputtered SiC samples have very similar fractured surfaces and porosities (Fig. 2).

Figure 3 shows SEM images of the ND containing SiC samples with varying compositions. Fluffy graphite can be observed in the grain boundary regions indicating that ND agglomerates transformed to graphite during the SPS treatment. The high-resolution SEM analysis shows no evidence of residual ND in the composites even at low sintering temperature (1600 °C). Fluffy graphite can still be detected on the fractured surfaces of the sample sintered at 1800 °C, but large graphite flakes are not visible. Based on the fractured surface analysis, we assume that the nanosized diamond (ND) transforms into nanographite or nanographene. The SEM observations also suggest that sputtered Si has no influence on the diamond → graphite transformation.

The fractured surface of the MD containing SiC samples sintered at 1600 °C (Fig. 4a) shows very similar structure to the SiC-ND composites. Thus, well-defined

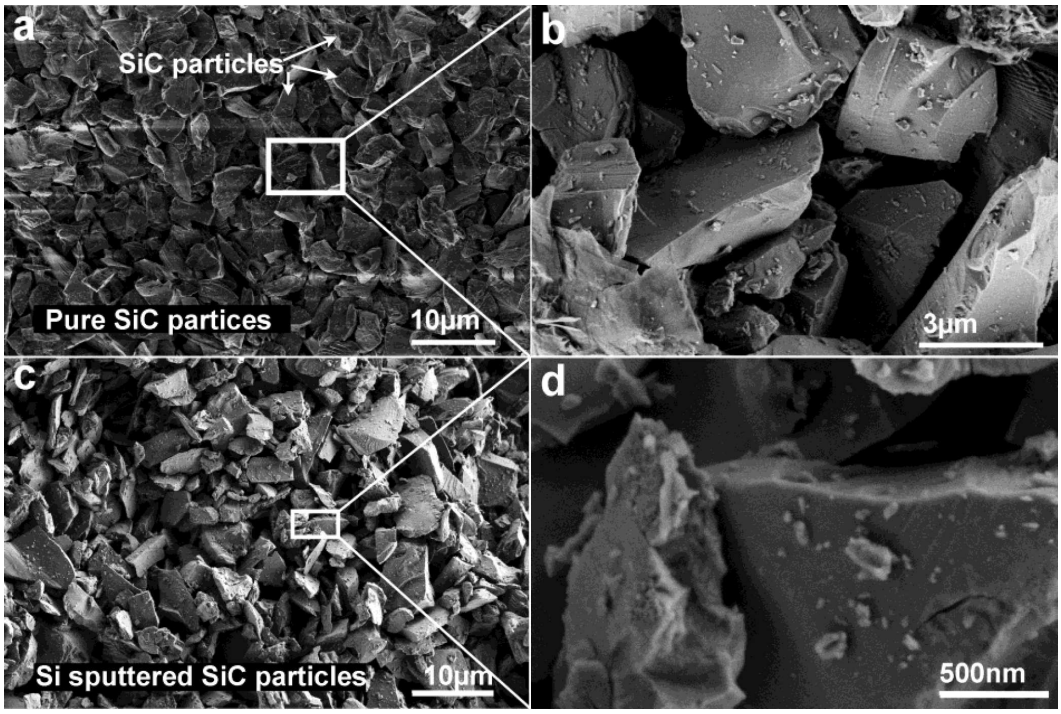

Figure 2. SEM micrographs of fractured surface of: a,b) the pure, diamond-free SiC and c,d) Si-sputtered, diamond free SiC samples

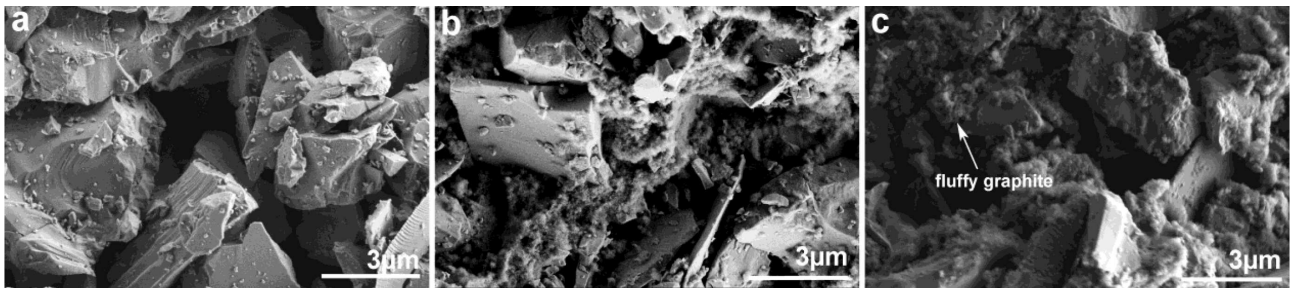

Figure 3. SEM micrographs of fractured surface of SiC-ND samples sintered at 1600 °C: a) Si-sputtered SiC sample, b) Si-sputtered SiC sample containing 10 wt.% ND and c) SiC sample containing 10 wt.% ND

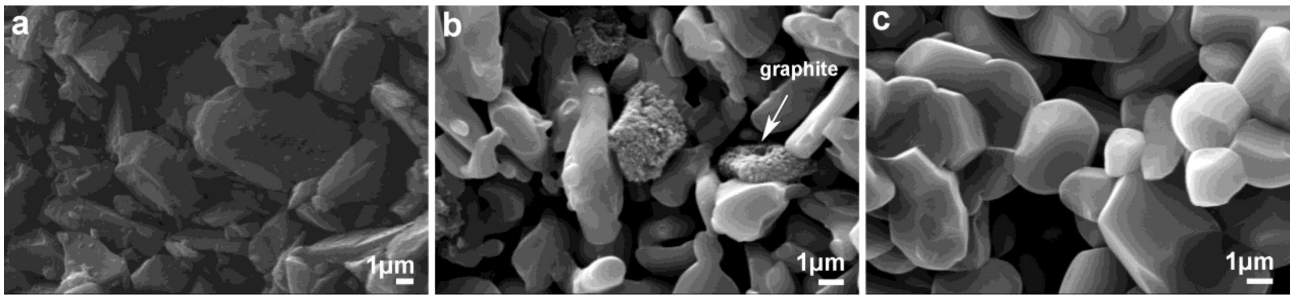

Figure 4. SEM micrographs of fractured surface of MD-SiC samples heat treated at: a) 1600, b) 1800 and c) 2000 °C

SiC particles with sharp edges occur, although the SiC-MD contains more Si than the SiC-ND samples. Increasing sintering temperature (1800 and 2000 °C) results in enlarged and rounded grains (Figs. 4b,c), which would indicate melting expected even at 1600 °C. The neck formations are formed between particles.

XRD data suggest that the SiC-MD composite sintered at 1600 °C still contains diamond. However, SEM images of the fractured surface do not provide a unique identification for diamond because the size and appearance of MD grains are very similar to SiC. Furthermore, Si particles are also indistinguishable, as it is assumed that they were melted during the SPS treatment and covered the composite SiC and MD particles.

For samples sintered at 1800 and 2000 °C temperature, the microstructural evaluation also confirms the MD → graphite transformation since graphite particle can be found in the composite (Fig. 4b). The microstructure analysis reveals, that despite the large amount of Si addition (10 wt.%) and large size of diamond particles, the sintered bodies show very porous structure, since the sintering process is not completed even at 2000 °C.

3.3. Evolution of the carbon structures

In order to study structural changes in the SiC-ND and SiC-MD composites Raman spectroscopy was used. Raman spectra of the initial SiC mixtures show the characteristic TO and LO bands of 6H SiC at ~775 and ~964 cm^{-1}, respectively (Fig. 5a). Our analysis confirms that the SiC TO band can be fitted with three peaks positioned at 755, 776 and 785 cm^{-1}, whereas the SiC LO band includes two peaks at 955 and 965 cm^{-1}. Although 4H-SiC was evidenced by XRD, its identification with Raman spectroscopy is inconclusive because the characteristic peaks of the 4H and 6H polytypes overlap at the 787 and 967 cm^{-1} positions.

The initial SiC-ND mixtures have the characteristic bands of Si and diamond at 520 and 1332 cm^{-1}, respectively (Fig. 5a). Furthermore, the SiC-MD mixtures are characterized by sharp diamond and lack of Si peaks. For the initial ND powder, there are two relatively intense and broad peaks at 1350 and 1587 cm^{-1} (the narrow diamond peak of small intensity sits on the former), which are characteristic for detonation-produced NDs [29] and can be associated with diaphite nanostructures [30] (Fig. 5b).

Figure 6a shows Raman spectra of the SiC-ND composites sintered at various temperatures. As a result of the high-temperature SPS heat treatment, the characteristic diamond band at 1332 cm^{-1} disappears and the broad features at 1350 and 1587 cm^{-1} become sharp and intensive (D-mode and G-mode) indicating the initial ND powder transformation to graphite. However, for the Si-sputtered SiC-ND system at low sintering temperature (1600 °C) the D-band is slightly shifted (~10 cm^{-1}) towards lower wavenumbers, which suggests the coexistence of sp^2 and sp^3 hybridized carbon structures. Raman spectra of the initial Si-sputtered powder mixture contain the characteristic band of Si. However, for the heated samples this band is not detectable. The high-

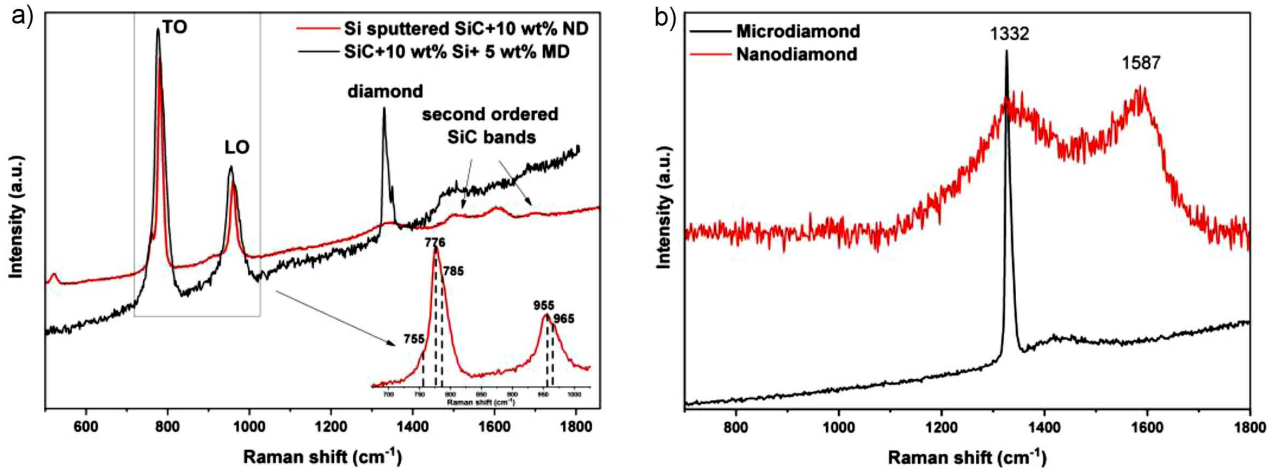

Figure 5. Raman spectra of: a) initial mixtures and b) raw diamond ND and MD powders

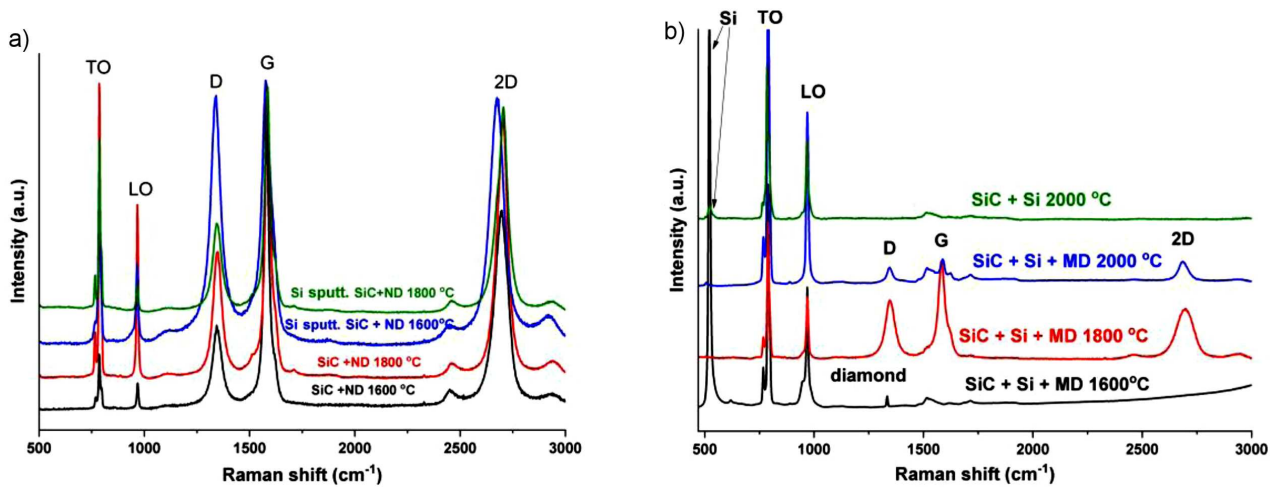

Figure 6. Raman spectra of: a) ND containing SiC and b) MD containing SiC samples sintered at various temperatures

temperature SPS treatment makes the appearance of TO and LO bands of SiC more complex. Our analysis suggests that the TO band contains well-separated peaks. However, we couldn't find correlation among the bands and the increasing sintering temperatures or Si additive.

The Raman spectra of the heat-treated MD containing SiC and reference samples are shown in Fig. 6b. The characteristic peaks of Si and MD are detectable in the sample sintered at 1600 °C. However, as the temperature increases the diamond peak slowly decreases and graphite peaks appear. These decreased amounts of Si can be associated with the inhomogeneous Si distribution, similar to what we observed from XRD data (Fig. 1b). In fact, the Raman investigation clearly demonstrates Si bands for the 10 wt.% Si containing MD-free SiC composite sintered at 2000 °C (Fig. 6b).

As a result of SPS treatment, the TO and LO bands of SiC are complex similar to the SiC-ND system. The TO band can be fitted with 4 peaks. Furthermore, in the samples heat-treated at 2000 °C new peak appears at 775 cm^{-1}, which can be unambiguously associated with the 4H-SiC polytype. This polytype has Raman peaks at 797 and 967 cm^{-1}, but they presumably overlap with those of 6H-SiC. For the samples sintered at 1600 °C the SiC LO band (at 970 cm^{-1}) has an asymmetric shape with a relatively intense shoulder at ~950 cm^{-1}, which can be attributed to the Fröhlich band arising from surface defects [31]. An alternative explanation of this peak is the second-order Raman mode of single crystal Si. As the sintering temperature increases the intensity of the shoulder decreases and it is undetectable for the sample treated at 2000 °C.

In order to obtain more information about the diamond → graphite transformation as the function of various composition and temperature, we analysed carefully the intensity ratio of graphite 2D and G bands (I_{2D}/I_G), from which the number of graphite layers can be determined. Table 2 shows the calculated intensity ratio of the 2D and G peaks for both SiC-diamond series. According to Ueda *et al.* [32] our calculated I_{2D}/I_G values suggest that diamond transformed to double layer graphene in the SiC-ND system. However, the I_{2D}/I_G ratio of the SiC + 10 wt.% ND sample sintered at 1600 °C imply the occurrence of multilayer graphene/nanographite. The high I_{2D}/I_G values of the SiC-MD sample imply the increase of graphite layer ordering. For the SiC-MD sample heat treated at 1600 °C the I_{2D}/I_G ratio could not be calculated because it does not contain graphite layer on diamond.

Our Raman investigation suggests that: i) both ND and MD diamond transform to graphite regardless of the Si content, ii) increasing temperature gives rise to higher ordering of graphite layers and iii) SiC does not form from Si and diamond.

3.4. Graphitization of prepared composites

In order to investigate the structure of the SiC-diamond system and the role of the bonding Si phase at high temperature, TEM analyses were performed. Thus, structure of the ND containing SiC sample sintered at 1600 °C is shown in Figs. 7a,b. The initial grain size (~2–5 μm) of SiC was preserved during heat treatment and the aggregated ND particles transformed to graphitic material. In particular, HRTEM images

Table 2. Calculated I_{2D}/I_G values of SiC-ND and SiC-MD composites

Compositions and sintering conditions			Raman I_{2D}/I_G ratio
ND-SiC composites	SiC + ND	1600 °C	1.4
	Si-sputtered SiC + ND	1600 °C	1.2
	SiC + ND	1800 °C	1.5
	Si-sputtered SiC + ND	1800 °C	1.5
MD-SiC composites	10 wt.% Si SiC + MD	1800 °C	1.1
	10 wt.% Si SiC + MD	2000 °C	1.3

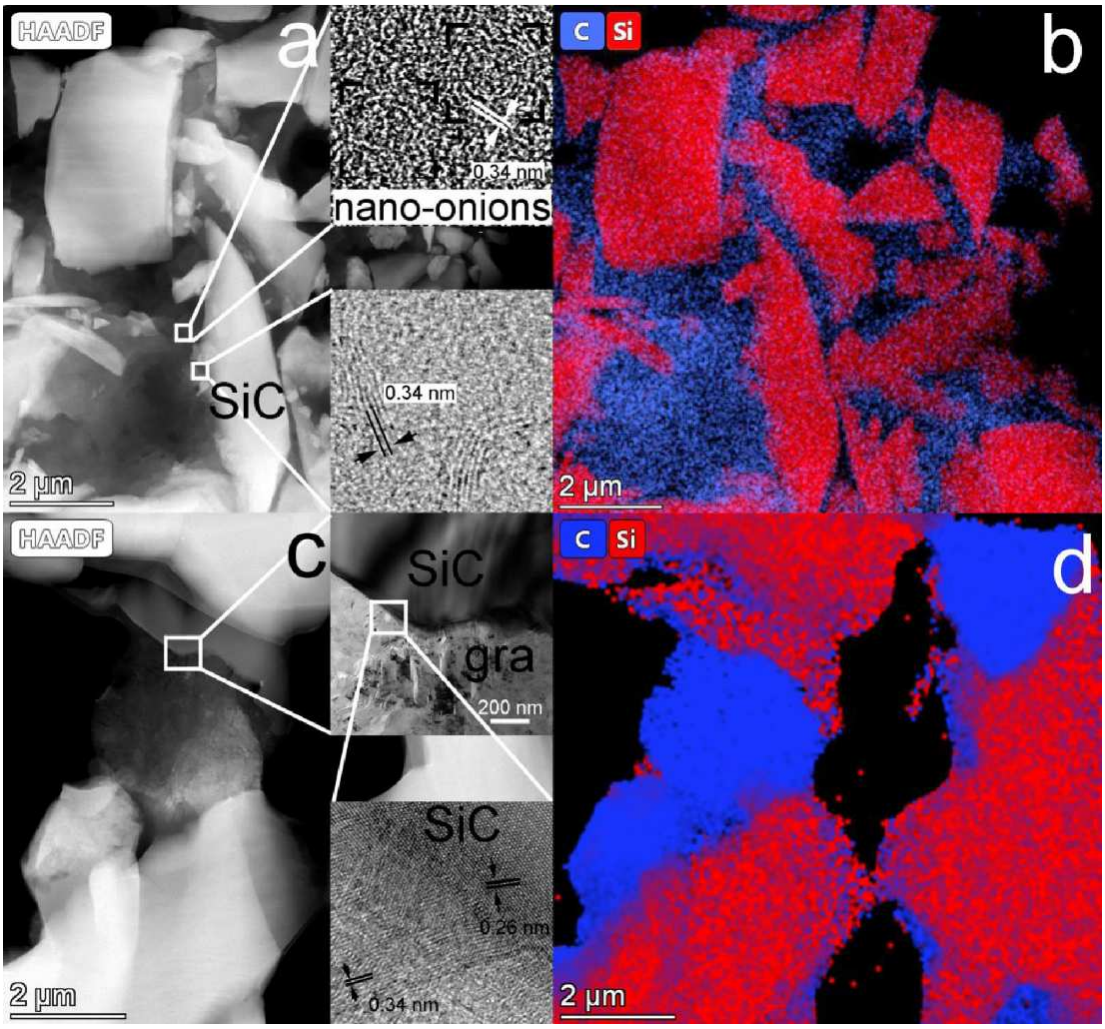

Figure 7. HAADF STEM image of ND-SiC with 1 wt.% Si sintered at 1600 °C (a), corresponding C and Si elemental maps (b), HAADF STEM image of MD-SiC with 10 wt.% Si sintered at 2000 °C (c) and corresponding C and Si elemental maps (d)

showed poorly ordered multi-shell carbon nano-onions and elongated few-layers graphene (Fig. 7a). We presume that these objects partially preserve the original morphology of the starting ND diamond. In fact, it has been proposed that NDs could reversibly transform to nano-onions [33,34]. Composite elemental map indicated the sample was poorly sintered (Fig. 7b).

In contrast with the ND-containing composite, the appearance of the graphite grains in the MD-containing SiC sample with 10 wt.% Si sintered at 2000 °C resembles the initial morphology and size of the MD diamond particles (Figs. 7c,d). During MD graphitization highly ordered graphite forms, similar to the observation of Zhang *et al*. [35]. In fact, there is no transitional phase between SiC and graphite and the graphite layers are almost parallel with the (001) SiC planes (Fig. 7c). Although abundant Si powder was added as a bonding material, our TEM measurement does not indicate its occurrence, which we explain with the inhomogeneous Si distribution. In summary the TEM study suggests that SiC does not form from Si and diamond even at high temperature, in contrast with the findings in the literature [14,20,21].

3.5. Presence of 5H-SiC polytype in composites

There are more than 200 polytypes of SiC [36], from which 4H and 6H are the most abundant with c_0 values of 10.061 and 15.130 Å, respectively. Although several studies report on the occurrence of an unusual 5H-SiC with the c_0 value of 12.584 Å, its identification is based on a single-crystal study [37] and an erroneously indexed JCPDS card (No. 42-1360). According to this card, 5H-SiC is characterized by the d values of 4.27 Å and 3.3 Å in comparison to 4H and 6H. However, these d values and the unindexed diffraction lines perfectly match those of quartz and the rest of the XRD peaks are consistent with that of 6H-SiC.

TEM is the best method for the identification of SiC polytypes because it provides an obvious image of the SiC stackings. Thus, HRTEM image (Fig. 8) unambiguously demonstrates the occurrence of periodic 5H-SiC in the MD-containing SiC sample sintered at 2000 °C. XRD data of this composite confirms presence of 6H-SiC (Fig. 1b). However, the broad peaks may also be consistent with 5H-SiC content because there is presumably small difference between the XRD data of these two polytypes. Since the HRTEM images of the SiC

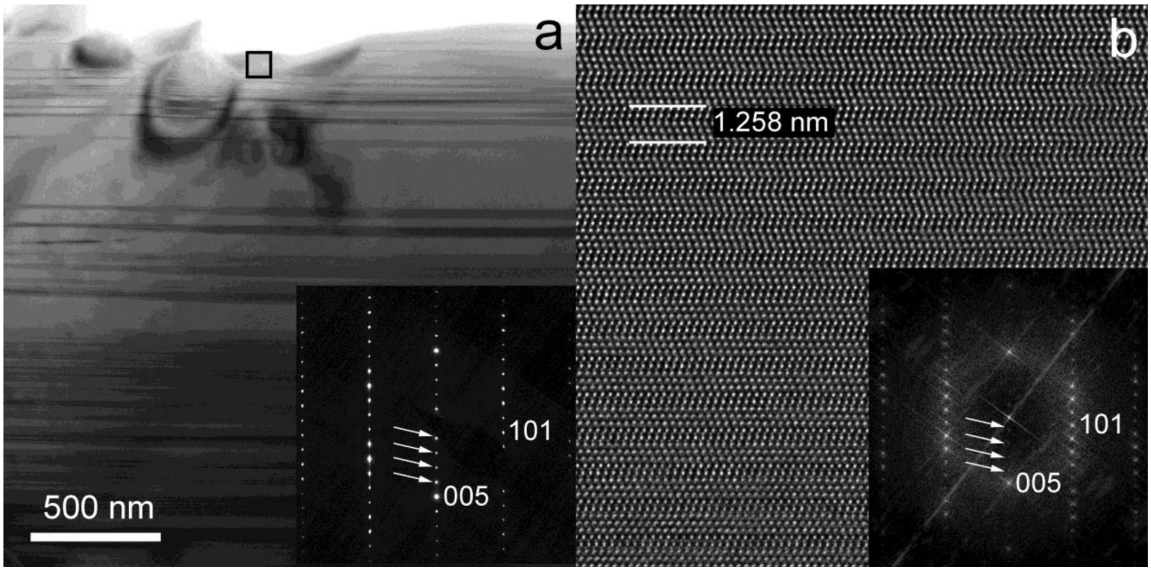

Figure 8. HFTEM image of an ion-bombarded area (a) and magnified image (b) -white arrows of the SAED pattern (a) and FFT (b) point to reflections arising from dynamically scattered electrons

samples heat-treated at 1600 and 1800 °C do not provide evidence for 5H-SiC, therefore, we suggest it is a high-temperature polytype. However, its application as a high-temperature indicator requires further study.

IV. Conclusions

SiC-Si-diamond composites were prepared by different types of diamond particles, nanocrystalline (ND) and microcrystalline (MD) diamond and sintered by high-temperature SPS method. XRD investigation confirmed that in the SiC-ND composites ND diamond transforms to nanographite even at low sintering temperature (1600 °C) and Si addition does not influence this transformation. The microstructure investigation showed fluffy nanographite in the composites matrix, and no evidence for large graphite flakes was found. The calculated Raman I_{2D}/I_G ratio values and the TEM images suggested that ND diamond transformed to nano-onions and few-layer graphene.

For the MD-containing SiC samples, XRD investigation indicated that diamond phase still exists after sintering at 1600 and 1800 °C. However, its amount decreased continuously with the increasing temperature, and at 2000 °C it transformed to graphite. Raman spectroscopy and TEM observations showed that with increasing sintering temperature the ordering of graphite is increased.

Our results suggested that ND and MD transform to graphite regardless of the Si and diamond content and quantity, and SiC does not form from the reaction of Si and diamond even at high temperature. Furthermore, the increasing sintering temperature resulted in highly-ordered graphite structure from diamond. It is intriguing that we identified 5H-SiC polytype in the composites quenched at 2000 °C. We clarified its occurrence and concluded that this polytype could presumably be associated with high-temperature heat-treatment.

Acknowledgement: The project was supported by the Hungarian National Research, Development and Innovation Office NKFIH_KH126502 and NKFIH_PD131848. We are grateful to the staff and for use of the HRTEM facility in Centre for Energy Research and the Raman facility in Wigner Research Centre for Physics established using grant VEKOP-2.3.3-15-2016-00002 and VEKOP-2.3.2-16-2016-00011 from the European Structural and Investments Funds, respectively. The authors thank to Noémi Szász for producing of the TEM samples and to Levente Illés for SEM measurements. P.N. acknowledges financial support from János Bolyai Research Scholarship and the ÚNKP-20-5-PE-7 New National Excellence program of the Ministry for Innovation and Technology. E. B. acknowledges financial support from János Bolyai Research Scholarship, as well.

References

1. A. Krueger, "Beyond the shine: Recent progress in applications of nanodiamond", *J. Mater. Chem.*, **21** [34] (2011) 12571–12578.
2. V.N. Mochalin, Y. Gogotsi, "Wet chemistry route to hydrophobic blue fluorescent nanodiamond", *J. Am. Chem. Soc.* **131**, [13] (2009) 4594–4595.
3. V.N. Mochalin, O. Shenderova, D. Ho, Y. Gogotsi, "The properties and applications of nanodiamonds", *Nat. Nanotechnol.*, **7** [1] (2012) 11–23.
4. G.R. Huss, "Meteoritic nanodiamonds: Messengers from the stars", *Elements*, **1** [2] (2005) 97–100.
5. S. Mitura, K. Mitura, P. Niedzielski, P. Louda, V. Danilenko, "Nanocrystalline diamond, its synthesis, properties and applications", *J. Achiev. Mater. Manuf. Eng.*, **16** [1-2] (2006) 9–16.
6. A.M. Schrand, S.A.C. Hens, O.A. Shenderova, "Nanodiamond particles: Properties and perspectives for bioapplications", *Crit. Rev. Solid State Mater. Sci.*, **34** [1-2] (2009) 18-74.

7. R. Kaur, I. Badea, "Nanodiamonds as novel nanomaterials for biomedical applications: Drug delivery and imaging systems", *Int. J. Nanomed.,* **8** (2013) 203–220.
8. A.S. Barnard, "Predicting the impact of structural diversity on the performance of nanodiamond drug carriers", *Nanoscale*, **10** [19] (2018) 8893–8910.
9. D. Kalyanasundaram, P. Molian, "Electrodeposition of nanodiamond particles on aluminium alloy A319 for improved tribological properties", *Micro Nano Lett.*, **3** [4] (2008) 110–116.
10. M. Ivanov, O. Shenderova, "Nanodiamond-based nanolubricants for motor oils", *Curr. Opin. Solid State Mater. Sci.*, **21** [1] (2017) 17–24.
11. W. Tillmann, M. Ferreira, A. Steffen, K. Rüster, J. Möller, S. Bieder, M. Paulus, M. Tolan, "Carbon reactivity of binder metals in diamond-metal composites - Characterization by scanning electron microscopy and X-ray diffraction", *Diam. Relat. Mater.*, **38** (2013) 118–123.
12. C. Xue, J.K. Yu, "Enhanced thermal conductivity in diamond/aluminum composites: Comparison between the methods of adding Ti into Al matrix and coating Ti onto diamond surface", *Surf. Coatings Technol.*, **217** (2013) 46–50.
13. Y. Mu, J. Guo, B. Liang, Q. Wang, "Rapid fabrication of the Ti_3SiC_2 bonded diamond composite by spark plasma sintering", *Int. J. Refract. Met. Hard Mater.*, **29** [3] (2011) 397–400.
14. M. Herrmann, B. Matthey, S. Höhn, I. Kinski, D. Rafaja, A. Michaelis, "Diamond-ceramics composites-New materials for a wide range of challenging applications", *J. Eur. Ceram. Soc.*, **32** [9] (2012) 1915–1923.
15. P. Németh, K. McColl, L. A.J. Garvie, C.G. Salzmann, M. Murri, P.F. McMillan, "Complex nanostructures in diamond", *Nat. Mater.*, **19** [11] (2020) 1126–1131.
16. P. Németh, K. Mccoll, R.L. Smith, M. Murri, L.A.J. Garvie, M. Alvaro, B. Pécz, A.P. Jones, F. Corà, C. G. Salzmann,. P. F. McMillan, "Diamond-graphene composite nanostructures", *Nano Lett.*, **20** [5] (2020) 3611–3619.
17. D.H. Yoon, I.E. Reimanis, "A review on the joining of SiC for high-temperature applications", *J. Korean Ceram. Soc.*, **57** (2020) 246–270.
18. E. Bódis, I. Cora, C. Balázsi, P. Németh, Z. Károly, S. Klébert, P. Fazekas, A.M. Keszler, J. Szépvölgyi, "Spark plasma sintering of graphene reinforced silicon carbide ceramics", *Ceram. Int.*, **43** [12] (2017) 9005–9011.
19. E. Bódis, Á. Fábián, K. Bán, Z. Károly, S. Klébert, A.M. Keszler, P. Fazekas, J. Szépvölgyi, "Microstructure and sintering mechanism of SiC ceramics reinforced with nanosized ZrO_2", *Eur. Chem. Bull.*, **6** [11] (2017) 484–490.
20. Y. Zhang, C.Y. Hsu, P. Karandikar, C. Ni, "Interfacial zone surrounding the diamond in reaction bonded diamond/SiC composites: Interphase structure and formation mechanism", *J. Eur. Ceram. Soc.*, **39** [16] (2019) 5190–5196.
21. C. Zhu, J. Lang, N. Ma, "Preparation of Si-diamond-SiC composites by in-situ reactive sintering and their thermal properties", *Ceram. Int.*, **38** [8] (2012) 6113–6136.
22. J. Qian, G. Voronin, T. W. Zerda, D. He, Y. Zhao, "High-pressure, high-temperature sintering of diamond-SiC composites by ball-milled diamond-Si mixtures", *J. Mater. Res.*, **17** [8] (2002) 2153–2160.
23. Y.S. Ko, T. Tsurumi, O. Fukunaga, T. Yano, "High pressure sintering of diamond-SiC composite", *J. Mater. Sci.*, **36** [2] (2001) 469–475.
24. G.A. Voronin, T.W. Zerda, J. Gubicza, T. Ungár, S.N. Dub, "Properties of nanostructured diamond-silicon carbide composites sintered by high pressure infiltration technique", *J. Mater. Res.*, **19** [9] (2004) 2703–2707.
25. J. Gubicza, T. Ungár, Y. Wang, G. Voronin, C. Pantea, T.W. Zerda, "Microstructure of diamond-SiC nanocomposites determined by X-ray line profile analysis", *Diam. Relat. Mater.*, **15** [9] (2006) 1452–1456.
26. T.P. Nguyen, Y. Pazhouhanfar, S.A. Delbari, Q. Van Le, S. Shaddel, A. Sabahi Namini, M. Shokouhimehr, M. Shahedi Asl, "Role of nano-diamond addition on the characteristics of spark plasma sintered TiC ceramics", *Diam. Relat. Mater.*, **106** (2020) 107828.
27. M. Fattahi, Y. Azizian-Kalandaragh, S.A. Delbari, A. Sabahi Namini, Z. Ahmadi, M. Shahedi Asl, "Nanodiamond reinforced ZrB_2–SiC composites", *Ceram. Int.*, **46** [8] (2020) 10172–10179.
28. S. Tóth, P. Németh, P. Rácz, L. Himics, P. Dombi, M. Koós, "Silicon carbide nanocrystals produced by femtosecond laser pulses", *Diam. Relat. Mater.*, **81** (2018) 96–102.
29. M. Mermoux, S. Chang, H.A. Girard, J.C. Arnault, "Raman spectroscopy study of detonation nanodiamond", *Diam. Relat. Mater.*, **87** (2018) 248–260.
30. P. Németh, K. McColl, L.A.J. Garvie, C.G. Salzmann, C.J. Pickard, F. Corà, R.L. Smith, M. Mezouar, C.A. Howard, P.F. McMillan, "Diaphite-structured nanodiamonds with six- and twelve-fold symmetries", *Diam. Relat. Mater.*, **119** (2021) 108573.
31. W. Lu, Y. Ou, E.M. Fiordaliso, Y. Iwasa, V. Jokubavicius, M. Syväjärvi, S. Kamiyama, P.M. Petersen, H. Ou, "With light emission for fluorescent SiC with porous surface", *Sci. Rep.,* **7** (2017) 9798.
32. K. Ueda, S. Aichi, H. Asano, "Direct formation of graphene layers on diamond by higherature annealing with a Cu catalyst" *Diam. Relat. Mater.*, **63** (2016) 148–152.
33. P. Németh, L.A.J. Garvie, "Extraterrestrial, shock-formed, cage-like nanostructured carbonaceous materials", *Am. Mineral.*, **105** [2] (2020) 276–281.
34. J. Xiao, G. Ouyang, P. Liu, C.X. Wang, G.W. Yang, "Reversible nanodiamond-carbon onion phase transformations", *Nano Lett.*, **14** [6] (2014) 3645–3652.
35. Y. Zhang, T. Wang, C. Y. Hsu, J. Wynn, P. Karandikar, J.P. Feser, C. Ni, "Thermal transport characteristics in diamond/SiC composites via molten Si infiltration", *Ceram. Int.*, **47** [12] (2021) 17084–17091.
36. N. Bernstein, H.J. Gotsis, D.A. Papaconstantopoulos, M.J. Mehl, "Tight-binding calculations of the band structure and total energies of the various polytypes of silicon carbide", *Phys. Rev. B - Condens. Matter Mater. Phys.*, **71** [7] (2005) 75203–75212.
37. N. Gnoevaja, L. Grozdanov, "Moissanite from Triassic rocks NW Bulgaria", *Proc. Bulg. Geol. Soc.*, **26** (1965) 89–95.